306–321 Nucleic Acids Research, 2022, Vol. 50, No. 1 Published online 14 December 2021
https://doi.org/10.1093/nar/gkab1205

The flip-flop configuration of the PABP-dimer leads to switching of the translation function

Sohyun Gu[1], Hyung-Min Jeon[1], Seung Woo Nam[1], Ka Young Hong[1], Md Shafiqur Rahman[1], Jong-Bong Lee[2,3], Youngjin Kim[1] and Sung Key Jang[1,2,*]

[1]Department of Life Sciences, Pohang University of Science and Technology, Nam-gu, Pohang 37673, Republic of Korea, [2]School of Interdisciplinary Bioscience & Bioengineering, Pohang University of Science and Technology, Nam-gu, Pohang 37673, Republic of Korea and [3]Department of Physics, Pohang University of Science and Technology, Nam-gu, Pohang 37673, Republic of Korea

Received July 01, 2021; Revised November 18, 2021; Editorial Decision November 20, 2021; Accepted November 23, 2021

ABSTRACT

Poly(A)-binding protein (PABP) is a translation initiation factor that interacts with the poly(A) tail of mRNAs. PABP bound to poly(A) stimulates translation by interacting with the eukaryotic initiation factor 4G (eIF4G), which brings the 3′ end of an mRNA close to its 5′ m^{7}G cap structure through consecutive interactions of the 3′-poly(A)–PABP-eIF4G-eIF4E-5′ m^{7}G cap. PABP is a highly abundant translation factor present in considerably larger quantities than mRNA and eIF4G in cells. However, it has not been elucidated how eIF4G, present in limited cellular concentrations, is not sequestered by mRNA-free PABP, present at high cellular concentrations, but associates with PABP complexed with the poly(A) tail of an mRNA. Here, we report that RNA-free PABPs dimerize with a head-to-head type configuration of PABP, which interferes in the interaction between PABP and eIF4G. We identified the domains of PABP responsible for PABP–PABP interaction. Poly(A) RNA was shown to convert the PABP–PABP complex into a poly(A)–PABP complex, with a head-to-tail-type configuration of PABP that facilitates the interaction between PABP and eIF4G. Lastly, we showed that the transition from the PABP dimer to the poly(A)–PABP complex is necessary for the translational activation function.

INTRODUCTION

The 5′ m^{7}G cap and 3′ poly(A) tail are known to synergistically stimulate translation by enabling mRNA circularization through the interaction between PABP and eIF4G (1–6). Findings from numerous studies have suggested that the poly(A) tail significantly enhances the translation of uncapped mRNAs, even though the extent of translational activation is weaker than that of mRNA containing the m^{7}G cap and poly(A) elements together (7–10). Interestingly, several reports have suggested that the m^{7}G cap-binding protein eIF4E is not a rate-limiting factor in general translation, despite its low expression level in cells (11–13). The depletion of eIF4E by 80–90% in various systems does not affect the global protein synthesis rate (11,12), but the translation of specific mRNAs involved in the regulation of reactive oxygen species requires eIF4E (13).

Considering the binding affinities of PABP to 3′ poly(A) (dissociation constant (K_D) = 0.67–7 nM) (14–17), PABP to eIF4G (K_D = 20 nM) (18), eIF4G to eIF4E (K_D = 34.5–74 nM) (19), eIF4E to the 5′ m^{7}G cap (K_D = 0.1–4.7 μM) (19–22), and the intracellular concentrations of the proteins (PABP, eIF4G (3-fold lower than that of PABP), and eIF4E (6-fold lower than that of PABP)) (14,23), it is most likely that translational initiation commences with the interaction between PABP and the poly(A) tail, followed by that between eIF4G and PABP-bound poly(A), between eIF4E and the eIF4G-PABP–poly(A) complex, and eventually between the 5′ m^{7}G cap and eIF4E-eIF4G-PABP–poly(A) complex, through interactions in the order of 3′-poly(A)–PABP-eIF4G-eIF4E-5′ m^{7}G cap. Therefore, the interactions between the poly(A) tail, PABP and eIF4G play pivotal roles in the initiation and regulation of translation in eukaryotic cells.

PABP is composed of four RNA-recognition motifs (RRMs) responsible for poly(A) binding and a hydrophobic C-terminal domain (CTD), which does not bind to RNA, composed of a linker region (designated as Linker) and MLLE (also known as PABC). Both RRMs and the PABP C-terminal domain are involved in the interaction with other proteins that modulate their translational function (24–26). For instance, PABP interacts with the scaffold protein eIF4G through RRM2 (26), which is crucial for the translational activation function of PABP. In contrast, PABP-interacting protein 2 (Paip2), which is a translation repressor, binds to two independent sites in RRM2-3

*To whom correspondence should be addressed. Tel: +82 54 279 2298; Fax: +82 54 279 8009; Email: sungkey@postech.ac.kr

and MLLE in PABP (24). Interestingly, several structural studies have revealed that PABP undergoes a major conformational change upon poly(A) binding, and its binding to partners is allosterically regulated (27–29). In addition to the crystal structure of linear human PABP RRM1-2 bound to poly(A)$_{11}$ complex (27), a single-molecule study has demonstrated that PABP undergoes a drastic conformational change in which linker2, present between RRM2 and RRM3, is sharply bent, leading to the positioning of RRM1 in close proximity of RRM4 in a single PABP molecule (28). The conformational change in PABP upon poly(A) binding was found to be necessary for the interaction with eIF4G and its translational activation function (17). In a recent study, the sharp bending of PABP upon binding to poly(A) was confirmed in the cryo-electron microscopy (cryo-EM) structure of yeast PABP–poly(A)$_{90}$ complex-associated Pan2-Pan3 deadenylase (29). Multiple PABP molecules are unidirectionally bound to poly(A) from 3′ to 5′, each molecule with a sharply bent conformation, which results in a zigzag conformation of the RNA–protein complex. The authors also showed that poly(A)-bound PABPs interact with each other in a head-to-tail configuration *via* interaction between RRM 1 and RRM 4 (Supplementary Figure S1). Collectively, previous reports have indicated that various conformations of PABP play important roles in the regulation of its function.

PABP is one of the most abundant proteins (∼4 μM in HeLa cells) (14). According to previous findings, most PABPs are not associated with poly(A) in cells as the molarity of mRNAs is ∼16-fold lower than that of PABP (14,30), and approximately two molecules of PABP are bound to an mRNA, considering the average length of the poly(A) tail of an mRNA (31,32). Therefore, only ∼13% of the total PABPs are estimated to be associated with poly(A), whereas approximately 87% of PABPs are not bound to poly(A). Even after considering the PABP regulatory proteins, such as Paip2 (present at concentrations 5–7-fold less than that of PABP) (33), a substantial quantity of PABPs is likely to remain in the free state in cells. The reason for the presence of free PABP molecules in abundance in cells and their role in translation are unknown. Several reports have shown that PABP overexpression in cells or the addition of excess recombinant PABP proteins to cell-free translation systems severely inhibits translation (17,34,35). The results suggest that the excess quantity of idling poly(A)-unbound PABPs exerts a negative impact on translation. Interestingly, the cellular concentration of eIF4G is ∼3-fold lower than that of PABP (23), which indicates that only approximately 30% of the total PABPs in cells are able to associate with eIF4G at most. In other words, eIF4G proteins can be sequestered to the abundant poly(A)-free PABPs if the idling PABPs bind to eIF4G as well as poly(A)-bound PABP. However, poly(A)-bound PABP exhibits a considerably higher affinity for eIF4G than poly(A)-unbound PABP (26), although the molecular basis for the preferential binding of eIF4G to mRNA-bound PABP, without competition with RNA-free PABPs present in large quantities, remains unknown. While the mechanism by which poly(A)-bound PABPs enhance translation has been studied extensively (35), neither the configuration of poly(A)-free PABPs nor the molecular basis of the poor interaction between eIF4G and poly(A)-free PABPs has been elucidated.

Here, we attempted to evaluate the molecular basis of the lack of interference by RNA-free PABPs in poly(A)-dependent translation through the potential sequestration of eIF4G. We found that RNA-free PABPs form a homodimer through a direct protein-protein interaction in the absence of poly(A). PABP dimer formation in an RNA-independent manner was confirmed not only using biochemical methods but also using cryo-EM. Moreover, we identified the domains of PABP required for direct PABP–PABP interaction using purified recombinant proteins. Lastly, we demonstrated the importance of the dynamic conversion of the PABP configuration in translation enhancement using a mutant PABP exhibiting stronger interaction activity between RNA-free PABPs than between wild-type PABP (PABP WT).

MATERIALS AND METHODS

Plasmids

The construction of pQE31-His-PABP-Flag has been described previously (17). His-PABP-Flag variants expressing RRM1-2–3–4 (residues 2–371), RRM1–2–3 (residues 2–299), RRM1-2 (residues 2–180), RRM2-3 (residues 97–299), RRM3-4 (residues 181–371), CTD (residues 372–636), Linker (residues 372–543), MLLE (residues 544–636), RRM2 (residues 97–175), RRM2-linker2 (residues 97–189), RRM3 (residues 190–299), and linker2-RRM3 (residues 176–299) were constructed as follows. The corresponding DNA regions were amplified using PCR with the plasmid pQE31-His-PABP-Flag as a template. The amplified DNA fragments were digested using NheI and BamHI and then inserted into the pET28a vector digested using NheI and BamHI. To construct GST-PABP, GST-RRM2-3 (residues 97–299), and GST-CTD (residues 372–636), the insert DNA was prepared by PCR amplification using pQE31-His-PABP-Flag as a template. The insert DNA digested using BamHI and XmaI was ligated with a BamHI- and XmaI-digested pGEX4T3 vector. To express 3 × FLAG-tagged PABP in mammalian cells, PABP cDNAs were amplified using PCR with pQE31-His-PABP-Flag as a template, digested with KpnI and BamHI, and then inserted into KpnI- and BamHI-digested pcDNA3.1–3 × Flag vector. Due to the technical issue of purifying full-length eIF4GI, His-eIF4GN, which is a truncated human eIF4GI N-terminus that contains PABP- and eIF4E-binding sites (residues 42–653 of eIF4GI) was used in the experiments (17). The construction of pET28a-His-eIF4GN and pGEX4T3-Paip2 has been described in a previous report (17). The constructs expressing PABP 4EA mutants of which four negatively charged glutamates (E) in the linker2 region (residues of E178, E180, E182 and E189) were substituted to alanines (A) were generated by site-directed mutagenesis from pQE31-His-PABP-Flag, pGEX4T3-PABP, and pcDNA3.1–3 × Flag PABP, respectively, using two common primers (forward, 5′-AGAACGAGAAGCTGAAGCTGGAGCTAGGGCAAAAG-3′; reverse, 5′-CTTTTGCCCTAGCTCCAGCTTCAGCTTCTCGTTCT-3′).

Protein expression and purification

His-PABP WT-Flag and His-PABP 4EA mutant-Flag were expressed in *Escherichia coli* M15 cells. Cells were cultured till an OD value of 0.3 was achieved, following which protein expression was induced by treatment with isopropyl-β-D-thiogalactopranoside (IPTG; 0.2 mM) for 24 h at 15°C. Various His-PABP variants, His-eIF4GN, and GST-fused proteins (GST-PABP WT, GST-PABP 4EA mutant, GST-CTD, GST-RRM2-3, GST, and GST-Paip2) were expressed in *E. coli* BL21 cells. Bacterial cells were cultured till an OD value of 0.5 was achieved, following which protein expression was induced by treatment with IPTG (1 mM) for 3 h at 37°C. Cells expressing His-tagged proteins (His-PABP WT-Flag, His-PABP 4EA mutant-Flag, His-tagged PABP variants, and His-eIF4GN) were lysed with lysis buffer A (50 mM Tris–HCl (pH 7.5), 300 mM NaCl, 1% Triton X-100, 5 mM β-mercaptoethanol, 20 mM imidazole, and 10% glycerol), and the proteins were purified with Ni-NTA beads (Qiagen). For purifying GST-fused proteins, the cells were lysed with lysis buffer B (50 mM Tris–HCl (pH 7.5), 300 mM NaCl, 1% Triton X-100, 5 mM β-mercaptoethanol, 1 mM reduced glutathione, and 10% glycerol), and the proteins were purified using glutathione-Sepharose 4B beads (GE Healthcare). The protein solutions were exchanged using dialysis buffer (10 mM HEPES–KOH (pH 7.5), 250 mM KCl, 1 mM $MgCl_2$, 0.1 mM EDTA, 1 mM DTT, and 10% glycerol) and aliquoted and stored after freezing in liquid nitrogen. Purified proteins used in the experiments were resolved by SDS-PAGE and visualized by Coomassie Blue staining (Supplementary Figure S2).

Estimation of protein size using size-exclusion chromatography (SEC)

His-PABP WT-Flag or His-PABP 4EA mutant-Flag proteins were loaded on a Superdex 200 10/300 GL column (GE healthcare) equilibrated with dialysis buffer. The size of PABP proteins was estimated based on the calibration curve created using the sizes of standard proteins (Supplementary Figure S3).

Preparation of cryo-EM grid and imaging

Purified His-PABP WT-Flag proteins were loaded onto a Superdex 200 Increase 10/300 column (GE Healthcare), and the fractions corresponding to the highest peak were collected. The proteins were concentrated to 0.19 mg/ml, and 4 μl of protein was applied to glow-discharged (0.39 mbar for 60 s) C-flat R1.2/1.3 (R1.2/1.3 400 meshes) grids. The grids were blotted for 3 s with a blot force of 2. The grids were vitrified into liquid ethane using Vitrobot Mark IV at 10 ºC under 100% humidity. Cryo-EM data were collected using a Talos Arctica microscope operated at 200 kV equipped with a Gatan K3 direct detector operating in the counted mode. A total of 1034 movies were recorded at a nominal magnification of 100 000×, corresponding to 0.83 Å/pixel at the specimen level. During data collection, images were acquired at a total exposure of 49.76 $e^-/A^{\circ 2}$ at the specimen level and evenly distributed over 50 frames for 3.23 s. A global defocus ranging from 0.8 to 2.8 mm was used as the preset target.

Cryo-EM image processing

The image stack in the counted mode was aligned using cryoSPARC 3.2.0 (36). The contrast transfer function (CTF) parameters of the micrographs were determined using CTFFIND4 (37). To obtain clear images, manual curation and sorting were performed, and ∼5000 particles over 100 micrographs were manually picked to generate templates for automatic picking. Initially, 100 228 particles were selected after automatic picking using cryoSPARC 3.2.0 (36). Several iterative rounds of two-dimensional (2D) classifications were performed to remove false pickings and classes with unclear features.

Electrophoretic mobility shift assay (EMSA)

A poly$(A)_{25}$ RNA (Bioneer) was 5′-end-labeled using the [^{32}P] radioisotope, and unincorporated radioisotopes were removed by phenol-chloroform extraction and ethanol precipitation. Radiolabeled RNAs were incubated with increasing concentrations of His-PABP WT-Flag or His-PABP 4EA mutant-Flag proteins for 15 min on ice in a binding buffer (20 mM Tris–HCl (pH 8.0), 70 mM KCl, 0.05% NP-40, 0.1 μg/μl BSA, 10% glycerol, and 1 mM DTT). The PABP–poly$(A)_{25}$ complex was resolved by electrophoresis in an 8% native polyacrylamide gel (acrylamide:bis-acrylamide ratio of 60:1) in pre-cooled 0.5× TBE at 200 V on ice. The gel was dried and analyzed by autoradiography (Amersham Typhoon 5).

Flag-immunoprecipitation and GST pull-down assay

For Flag-immunoprecipitation, FLAG-antibody-conjugated beads (Sigma) were prepared by washing once with ice-cold immunoprecipitation buffer (40 mM HEPES–KOH (pH 7.5), 100 mM KCl, 1 mM EDTA, 10 mM β-glycerophosphate, 10 mM NaF, 2 mM Na_3VO_4, 1% NP-40 and 1 mM PMSF). Flag-tagged PABP was incubated with the beads for 30 min at 4°C. After washing the beads once, GST-PABP or His-eIF4GN proteins were added to the bead solution and further incubated for 30 min at 4°C. The beads were washed five times with ice-cold immunoprecipitation buffer, and the bead-bound proteins were eluted by adding sample buffer and boiling. The proteins were resolved using SDS-polyacrylamide gel electrophoresis (SDS-PAGE) and analyzed using Western blotting. For immunoprecipitation with mammalian cell extracts, as shown in Figure 1D, Huh-7 cells were lysed with ice-cold immunoprecipitation buffer. Cyanase (RiboSolutions) (or an equal volume of immunoprecipitation buffer) was added to the whole cell extract (WCE) and incubated for 30 min at 37°C. WCEs were pre-cleared with Protein-G Agarose resin (Roche) for 1.5 h at 4°C and then incubated with Flag-antibody-conjugated beads (Sigma) for 2 h at 4°C under continuous rotation. The beads were washed three times with immunoprecipitation buffer, and the bead-bound proteins were eluted, resolved using SDS-PAGE, and analyzed by Western blotting. To confirm the digestion of endogenous RNAs using cyanase, RNAs from each input sample were extracted using TRI-Solution (Bio Science Technology) according to the manufacturer's instructions and loaded on a 1% agarose gel. The GST

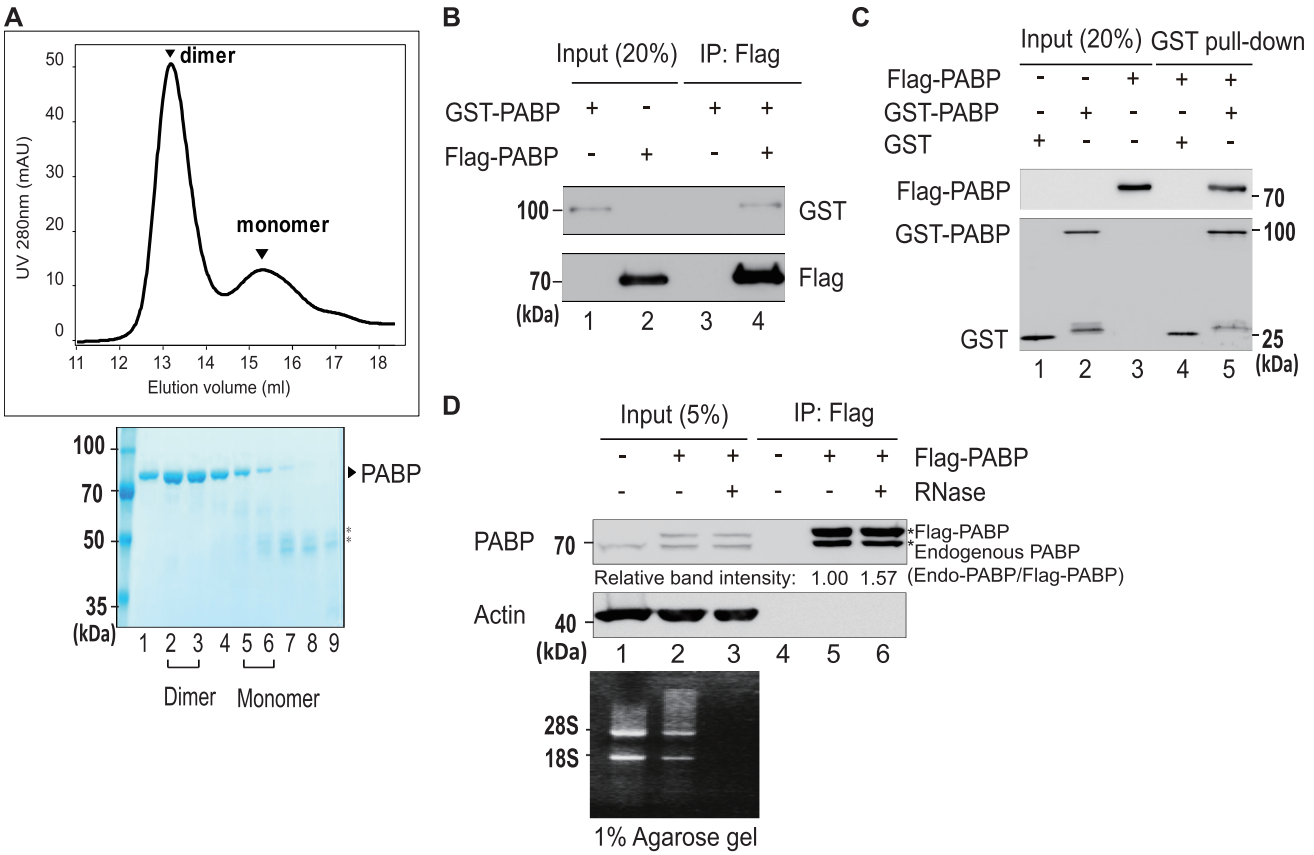

Figure 1. PABP forms a homo-dimer through a direct protein-protein interaction. (**A**) Size exclusion chromatography was carried out with Flag-PABP proteins. Purified Flag-PABP proteins (4 μM) were injected into a Superdex 200 10/300 GL column (GE healthcare). Upper panel: Gel filtration profile of PABP proteins. The positions of dimeric and monomeric PABPs are depicted by arrowheads. Lower panel: The proteins in each fraction resolved by 10% SDS-PAGE and stained by Coomassie Blue. The bands depicted by asterisk (*) are likely either bacterial proteins co-purified with PABP or fragment(s) of PABP generated during the purification steps. (**B**, **C**) The physical interaction between Flag-PABP and GST-PABP protein was investigated by (B) Flag-immunoprecipitation and (C) GST pull-down experiments. Western blot analyses were performed with anti-Flag (to detect Flag-PABP) and anti-GST (to detect GST-PABP) antibodies. (**D**) Confirmation of PABP–PABP interaction using cells. Flag-immunoprecipitation was performed with Huh7-cells expressing 3x Flag-PABP to detect endogenous PABP with or without treatment of an RNase cyanase. Endogenous PABPs co-precipitated with Flag-PABPs were monitored by Western blotting using an anti-PABP antibody (upper panel). The level of endogenous PABP was quantified and normalized to the level of Flag-PABP in each lane. Actin was used as a negative control of non-specific binding of endogenous proteins with Flag resin or Flag-PABP conjugated resin. Degradation of endogenous RNAs by the treatment of cyanase was confirmed by agarose gel electrophoresis of RNAs isolated from input samples (lower panel).

pull-down assay was performed in a manner similar to Flag-immunoprecipitation, except that GST-tagged proteins were pre-incubated with glutathione-Sepharose 4B beads (GE Healthcare) before Flag-tagged proteins were added into the bead solution.

Poly(A) pull-down assay

Poly(A) sepharose-4B beads (GE Healthcare) were prepared as previously described (17). His-PABP WT-Flag or His-PABP 4EA mutant-Flag proteins were incubated with the beads for 30 min at 4°C, and the beads were washed once with ice-cold immunoprecipitation buffer. His-eIF4GN proteins were added and incubated for 30 min at 4°C, following which the beads were washed with ice-cold immunoprecipitation buffer three times. The beads were boiled with sample buffer, and the proteins were subjected to SDS-PAGE and analyzed using Western blotting.

In vitro translation using PABP-depleted rabbit reticulocyte lysate (RRL)

Nuclease-untreated RRL was purchased from Promega. The lysates were incubated with GST-Paip2-conjugated glutathione-Sepharose 4B beads (GE Healthcare) to deplete endogenous PABP, as described previously (38). For controls, the same quantity of lysate was incubated with GST-conjugated glutathione-Sepharose 4B beads. m^7G capped and poly(A)$_{120}$-tailed mRNAs containing the *Renilla* luciferase gene were synthesized *via in vitro* transcription. *In vitro* translation was performed using the mRNAs (final concentration, 5 nM) in control or PABP-depleted lysates supplemented with increasing concentrations of His-PABP WT or PABP 4EA mutant proteins (25–100 ng). The *in vitro* translation mixtures were incubated at 30°C for 20, 40, 60 and 80 min, and luciferase activities were measured to assess the translation efficiency.

Cell culture

Huh-7 cells were cultured in Dulbecco's modified Eagle's medium (Gibco BRL) supplemented with 10% fetal bovine serum (PEAK) and 1% penicillin/streptomycin.

Cell transfection and luciferase assays

Cells with an approximate confluency of 70% were transfected with a negative control siRNA and 3′ untranslated region (3′UTR)-targeting siRNAs (CCUUAUGUACCGAGCAAAU = UU (sense); AUUUGCUCGGUACAUAAGG = UU (anti-sense)) or PABP coding-region-targeting siRNA #1 (Bioneer) (39) using Lipofectamine 3000 (Invitrogen) according to the manufacturer's instructions. After 48 h of incubation, the cells were re-transfected with a reporter DNA encoding *Renilla* luciferase (100 ng) and various quantities of effector DNA encoding WT PABP or the mutant PABP 4EA. At 24 h after the second transfection, the cells were lysed using ice-cold immunoprecipitation buffer, and the *Renilla* luciferase activity in the cell extracts was measured. To normalize the transfection efficiency of reporter DNA in each well, total RNA from the cell lysates was extracted using TRI-Solution (Bio Science Technology) according to the manufacturer's instructions. The levels of *Renilla* luciferase and *GAPDH* mRNA were measured *via* quantitative PCR with the LightCycler 480 system (Roche) using the following primers: *Renilla* forward, 5′-TGTGCCACATATTGAGCCAG-3′; *Renilla* reverse, 5′-CCAAACAAGCACCCCAATCA-3′; *GAPDH* forward, 5′-GTCTCCTCTGACTTCAACAGCG-3′; *GAPDH* reverse, 5′-ACCACCCTGTTGCTGTAGCCAA-3′. The MIQE (40) checklist is provided in Supplementary Table S1.

RESULTS

PABPs form homodimers in the absence of RNA

PABP molecules are known to consecutively bind to the 3′ poly(A) tail of mRNAs, which leads to the formation of a long chain of proteins associated with an mRNA; however, the configuration of RNA-free PABP molecules remains unknown. To investigate whether RNA-free PABPs also form a protein complex similar to that formed by poly(A)-associated PABPs, we synthesized and purified recombinant PABP proteins containing a 6× His-tag at the N-terminus and a 3× Flag-tag at the C-terminus (hereafter referred to as Flag-PABP). PABP was treated with RNase A during purification to minimize potential contamination by endogenous PABP-associated *E. coli* RNAs. The size of PABP was estimated by SEC with purified proteins (Figure 1A). Surprisingly, the size of PABP estimated according to the major, prominent peak (13.37 ml) in SEC was approximately 151 kDa, which was approximately double the apparent molecular weight of monomeric PABP (73 kDa) (Supplementary Figure S3). Additionally, a minor peak (15.65 ml estimated to be 56 kDa) was also observed, which was most likely the peak of monomeric PABPs (Figure 1A). No peak was observed for larger-sized PABPs (trimer or larger oligomer) in the chromatograph. The results indicate that the majority of PABP proteins exist in the dimeric form in the absence of their binding counterpart, i.e. the poly(A) tail of an mRNA. The proteins in each fraction (0.5 ml) were analyzed using SDS-PAGE and Coomassie Blue staining. Most PABP molecules were eluted in the dimer fraction (13–14 ml, lanes 2 and 3 in Figure 1A, lower panel), whereas a small quantity of PABP molecules was detected in the monomer fraction (14.5–15.5 ml, lanes 5 and 6). Some proteins smaller than PABP (denoted by * on lanes 6–9 in Figure 1A, lower panel) were detected. These proteins were most likely PABP fragments or the bacterial proteins co-purified with PABP. Therefore, the considerable height of the monomeric peak of monomeric PABP in the upper panel of Figure 1A was attributed to the contaminating proteins present in fractions 5 and 6. The ratios of dimeric to monomeric PABP proteins, which were measured by the band intensities of PABP in the gel, were the same (9:1) at various PABP concentrations near the physiological one (4 μM). This may indicate that the RNA-free PABPs are in equilibrium between monomers and dimers in favor of dimerization at physiological conditions (Supplementary Figure S4).

To confirm the protein-protein interaction between RNA-free PABP molecules, we performed co-immunoprecipitation (Co-IP) experiments using two PABP variants with different tags (GST- and Flag-tags). We cloned and purified both Flag-tagged and GST-tagged PABP proteins and performed Co-IP experiments using a Flag antibody-conjugated resin (Figure 1B) or a Glutathione Sepharose 4B resin (Figure 1C). As shown in Figure 1B, GST-PABP protein co-precipitated with the Flag-PABP protein but not with the negative control (comparing lane 4 with lane 3 in Figure 1B). Conversely, Flag-PABP co-precipitated with GST-PABP, but not with the negative control GST (comparing lane 5 with lane 4 in Figure 1C). Collectively, the SEC and Co-IP results indicate that RNA-free PABP proteins form homodimers through direct protein–protein interactions.

In addition, we evaluated the interaction between RNA-free PABPs in cell extracts treated with a non-specific endonuclease (cyanase) that degrades all cellular nucleic acids. We performed Co-IP experiments using cell extracts from Huh-7 cells ectopically expressing Flag-PABP (Figure 1D). Flag-PABP was precipitated with a Flag antibody-conjugated resin, following which both Flag-PABP and endogenous PABP proteins co-precipitated by Flag-PABP were visualized by Western blotting with a PABP antibody. As shown in lanes 5 and 6 in Figure 1D, not only Flag-PABP but also endogenous PABP proteins were precipitated in the resin-associated protein pool. Of note, Flag-PABP is slightly larger than endogenous PABP owing to the addition of the 3× Flag tags. The removal of cellular RNA was confirmed by agarose gel electrophoresis (Figure 1D, lower panel). The results also indicate that the PABP–PABP complex is formed by direct protein-protein interaction without assistance from poly(A) RNA. Moreover, this result strongly supports the formation of RNA-free PABP homodimers, which was demonstrated using purified PABP proteins, as shown in Figure 1A.

The linker2-RRM3 and linker in CTD of PABP participate in RNA-free PABP–PABP interaction

Several reports have suggested that the CTD of PABP plays a role in cooperative binding to poly(A) by promoting intermolecular interactions between PABP molecules (15,41,42). Using EMSA (15,41) or nanopore assays (42), the authors suggested that the CTD participates in the PABP–PABP interaction, since they observed the abrogation of the cooperative binding of PABP molecules to a long poly(A) stretch upon the deletion of the CTD sequence. Other attempts have been made to identify the protein-protein interaction domain in PABP molecules using [^{35}S]-labeled PABP generated *via in vitro* translation in RRLs (41,43). The authors attempted to identify the domains responsible for the PABP–PABP interaction in co-precipitation experiments using various deletion mutants of GST-PABP (or His-PABP) and [^{35}S]-labeled PABP generated in RRL (41,43). However, the results were contradictory, even though the approaches were considerably similar in principle (see below). The reason for this discrepancy remains unclear. We speculate that the discrepancy could be attributed to the difference in the protein-binding conditions, the presence or absence of poly(A)-tailed mRNAs, and/or the presence of endogenous proteins in RRL that interact with PABP directly or indirectly.

To identify the domains responsible for PABP–PABP dimer formation in the absence of poly(A) RNA, we generated and purified PABP variants spanning different parts of PABP without contaminating proteins or RNAs. The PABP variants contain either a Flag-tag or GST-tag to facilitate the purification and detection of the proteins *via* affinity chromatography or Western blotting, respectively. The PABP variants were expressed in *E. coli*. We generated GST-tagged full-length PABP and Flag-tagged PABP variants, as depicted schematically in Figure 2A. The interactions between Flag-tagged PABP variants and GST-tagged full-length PABP (GST-PABP (1–2-3–4-C)) were assessed using Co-IP with a Flag antibody-conjugated resin. As shown in Figure 1B, GST-PABP was co-precipitated with Flag-1–2-3–4-C (2–636), but not with the negative control Flag resin (compare lane 10 with lane 9 in Figure 2B). GST PABP was co-precipitated with Flag-1–2-3–4 (2-371), Flag-1–2–3 (2–299), Flag-2–3 (97–299), and Flag-C (372–636), but not with Flag-1–2 (2–180) or Flag-3–4 (181–371) (lanes 11 to 16 in Figure 2B). Of note, full-length PABP can interact with at least two independent regions of PABP, one of them being domain 2–3, the common segment in domains 1–2–3–4, 1–2–3, and 2–3, which showed positive signals in Co-IP experiments (lanes 11, 12 and 14 in Figure 2B). Domain 2–3, which showed a positive signal, contain an additional region named linker2 compared to domains 1–2 and 3–4, which showed no signals in Co-IP experiments (lanes 13 and 15 in Figure 2B). The results indicate that individually, domains 2 and 3 were unsuitable for the PABP–PABP interaction. We also found that domain C contains an independent PABP–PABP interaction domain (lane 16 in Figure 2B), but the binding affinity is much weaker than that of domain 2–3 (compare lane 14 with lane 16 in Figure 2B). The results indicate that the interaction through domain 2–3 and CTD play the major and minor roles, respectively, in the PABP–PABP interaction.

We further investigated whether domain 2–3 interacts with domain 2–3 or domain C using GST-tagged domain 2–3 (GST-2–3) and GST-tagged domain C (GST-C) sequences, respectively. GST-C co-precipitated with Flag-C, but not with Flag-1–2–3–4 (Figure 2C). Conversely, GST-2–3 co-precipitated with Flag-1–2–3–4, but not with Flag-C (Figure 2D). The results indicate that the RRM domains interact with RRM domains and the CTD interacts with the CTD. In other words, PABP forms a dimer through head-to-head interaction in the absence of RNA. We further attempted to identify the site responsible for the RRM-to-RRM interaction in PABP. We performed Co-IP with GST-2–3 and truncated variants of PABP named Flag-1–2, Flag-2–3, and Flag-3–4 (Figure 2E). GST-2–3 was found to interact with Flag-2–3 (lane 13 in Figure 2E) as well as Flag-1–2–3–4 (lane 11 in Figure 2E). Unexpectedly, Flag-3–4 was also slightly precipitated with GST-2–3 (lane 14 in Figure 2E), although to a much lesser extent than Flag-2–3 (see below). Conversely, Flag-1–2 did not precipitate with GST-2–3 (lane 12 in Figure 2E).

We further attempted to identify the essential regions in RRM2–3 and CTD required for the PABP–PABP interaction. RRM2-3 was divided into four subparts (RRM2, RRM2-linker2, RRM3, and linker2-RRM3), and the protein-protein interactions between RRM2-3 and the subparts was tested using Co-IP with a Flag antibody-conjugated resin (Supplementary Figure S5). The linker2 sequence is present in the region between RRM2 and RRM3, spanning amino acids 176 to 189. GST-2–3 co-precipitated with Flag-linker2-RRM3 (176–299) (lane 12 in Supplementary Figure S5B) as well as Flag-RRM2-3 (97–299) (lane 8 in Supplementary Figure S5B), but not with the three other variants Flag-RRM2 (97–175), Flag-RRM2-linker2 (97–189) and Flag-RRM3 (190–299) (lanes 9–11, Supplementary Figure S5B). The results suggest that the region spanning linker2-RRM3 is necessary and sufficient for the PABP–PABP interaction, whereas RRM2 is not necessary for this interaction. Of note, as shown in Figure 2E, Flag-RRM3-4 contain a part of the linker2 region (amino acids 181–189) at the N-terminal end of RRM3-4. We expect that the partial linker2 region likely contributes to the weak interaction of Flag-RRM3-4 with GST-RRM2-3, as shown in Figure 2E. CTD was divided into two subparts (Linker and MLLE), and the protein-protein interactions between CTD and the subparts was tested using Co-IP with a Flag antibody-conjugated resin (Supplementary Figure S6). GST-C co-precipitated with Flag-Linker (372–543) (lane 7 in Supplementary Figure S6B) as well as Flag-C (372–636) (lane 6 in Supplementary Figure S6B), but not with Flag-MLLE (544–636) (lane 8 in Supplementary Figure S6B). The results indicate that the Linker in CTD is necessary and sufficient for the interaction between CTDs. Collectively, our data suggest that PABP homodimerization is mediated by two independent domains: linker2-RRM3 and the Linker in CTD. The PABP homodimer model with a head-to-head configuration, which was hypothesized from our findings, is depicted in Figure 2F.

We attempted to determine the cryo-EM structure of RNA-free PABPs to validate our PABP homodimer model (Figure 2G). We isolated RNA-free PABP dimers using size exclusion chromatography (Figure 1A) and performed cryo-EM for structural analysis. Using 2D classification, we

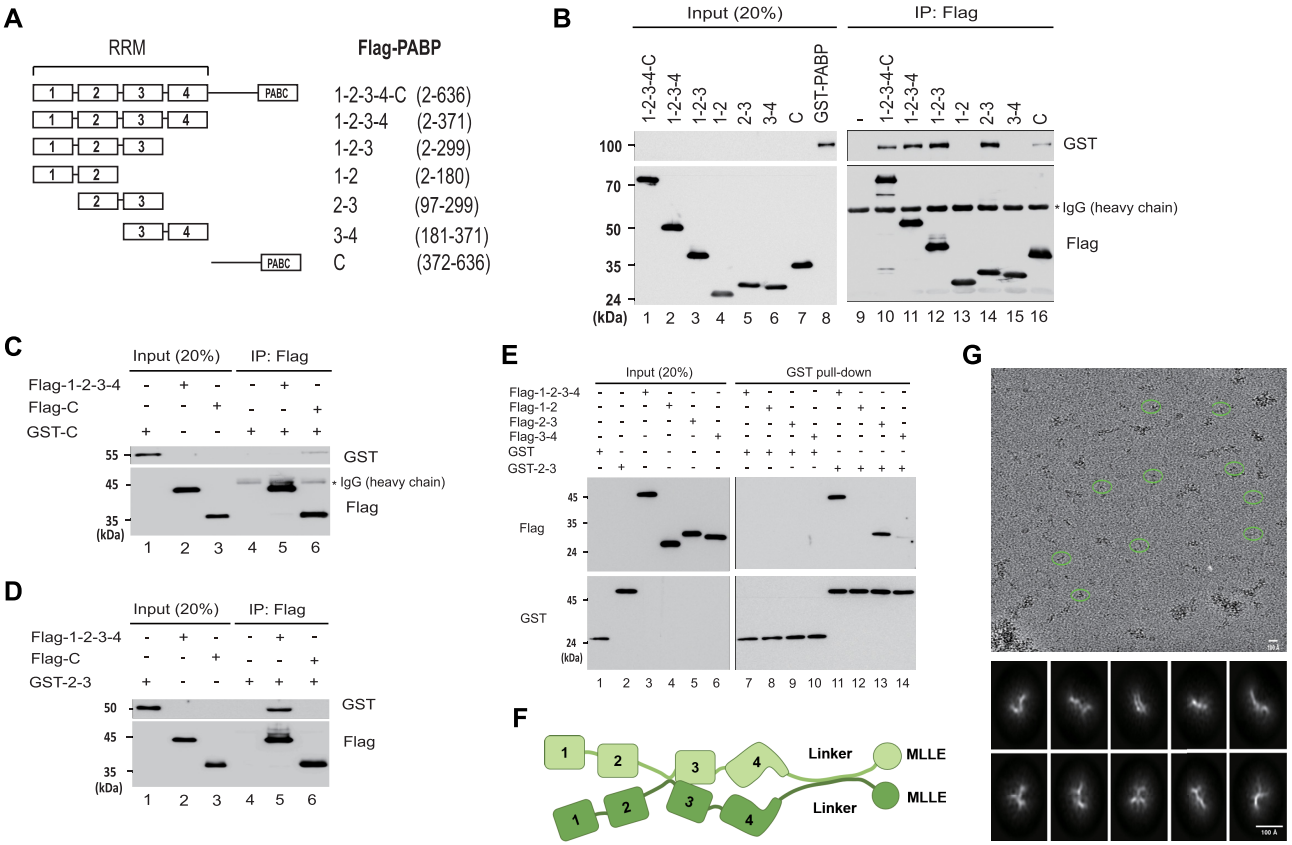

Figure 2. Determination of domains in PABP required for the PABP–PABP interaction. (**A**) Schematic diagram of Flag-tagged PABP and its variants with deletion mutations. (**B**) Co-immunoprecipitation of GST-tagged full-length PABP with Flag-tagged PABP variants. Flag-PABP variants and GST-PABP mixtures were incubated and precipitated by a Flag antibody-conjugated resin. The resin-bound proteins were visualized by Western blotting using the indicated antibodies. (**C**) Interaction between C-terminal domain and C-terminal domain of PABP. Flag-1–2–3–4 (2-371) or Flag-C (372–636) proteins were incubated with GST-C (372–636) proteins and a Flag antibody-conjugated resin. The resin-bound proteins were visualized by Western blotting using the indicated antibodies. **(D)** Interaction between RRM2-3 (97–299) and RRM1-2–3–4 (2–371) of PABP. GST-2–3 (97–299) protein was incubated with Flag-1–2–3–4 (2–371) or Flag-C (372–636) protein and a Flag antibody-conjugated resin. The resin-bound proteins were visualized by Western blotting using the indicated antibodies. (**E**) Interaction between RRM2-3 (97–299) and RRM2-3 (97–299) of PABP. GST pull-down assays were performed with GST (lanes 7–10) or GST-2–3 (97–299) proteins (lanes 11–14) to pull-down Flag-tagged PABP truncation mutants [Flag-1–2–3–4 (2–371), Flag-1–2 (2–180), Flag-2–3 (97–299), and Flag-3–4 (181–371)]. The resin-bound proteins were visualized by Western blotting using the indicated antibodies. (**F**) A schematic drawing of PABP homo-dimer with a head-to-head orientation. RNA-free PABPs form a homo-dimer by interaction through two independent domains of 1) linker2-RRM3 and 2) C-terminal domain. (**G**) Cryo-EM structure of RNA-free PABP proteins. (Upper panel) Representative micrograph images of RNA-free PABPs in C-flat grids after motion correction and dose weighting. After motion correction, contrast transfer function (CTF) estimation was performed to discard poor images. The motion correction was performed by full-frame motion correction with cryoSPARC (36), and CTF was estimated by using CTFFIND4 (37). Micrograph image size is 4096 × 5760 pixel size (0.83 Å/pixel). (Lower panel) 2D classification from finally yielded images. A total of 1034 micrographs were analyzed. Five classes in the upper row represent thread-shaped 2D classes of PABP particles. The thread shaped classes, especially the third class, look like two threads are aligned in a head-to-head configuration. Five classes in the lower row represent 2D class of PABP particles with a butterfly-shape with the central parts associated together.

found that RNA-free PABP proteins form a thread-like (upper row of lower panel in Figure 2G) or a butterfly-like conformation (lower row of lower panel in Figure 2G). Among the thread-shaped 2D PABPs, some molecules showed two threads aligned in a head-to-head (or tail-to-tail) configuration, whereas among the butterfly-shaped PABPs, the middle parts of the molecules were found to associate with each other while the N- and C-terminal ends remained flexible. We speculate that the middle region of the two RNA-free PABPs are connected to each other through the interaction between the linker2-RRM3s of PABP, whereas the N- and C-terminal ends remain flexible as they do not interact with each other and move freely. The interaction between CTDs may not be observed in the structural analysis, possibly owing to the weak binding affinity and the unstructured nature of the domain (44). The flexible nature of RNA-free PABP was previously demonstrated using single-molecule fluorescence resonance energy transfer technology (28). Although we could not determine the three-dimensional structure of RNA-free PABP at high resolution owing to its highly flexible nature, we could confirm that RNA-free PABPs form a homodimer *via* a connection in the middle region not only using biochemical methods but also using the cryo-EM technique.

The PABP homodimer dissociates upon binding to poly(A) RNA

As described above, PABP strongly binds to poly(A) RNA at a sub-nanomolar range of K_D values (14–17), and a drastic conformational change is induced at the linker2 region between RRM2 and RRM3 upon the binding of poly(A) RNA (28). Since linker2-RRM3 also participates in the PABP–PABP interaction as shown in Figure 2 and Supplementary Figure S5, we investigated the effect of poly(A)–PABP binding on the PABP–PABP interaction. We performed Co-IP experiments using GST-PABP and Flag-PABP proteins in the presence of increasing concentrations of poly(A)$_{25}$ RNA (Figure 3A). In the experiments, we used poly(A) RNA containing 25 adenosine monophosphates that allowed the binding of only one PABP molecule (45) to exclude the experimental complications attributed to PABP–PABP interaction(s) among the molecules associated with a long poly(A) RNA. After pre-incubation of the GST-PABP and Flag-PABP proteins with Flag-conjugated beads, we added increasing concentrations of poly(A)$_{25}$ till the concentration was equal to the sum of the concentrations of GST-PABP and Flag-PABP proteins (referred to as 1×). The gradual inhibition of the PABP–PABP interaction was observed in response to the increase in poly(A)$_{25}$ concentration (comparing lanes 4 to 7 in Figure 3A), indicating that poly(A)$_{25}$ inhibits the homodimerization activity of PABP. We speculate that the drastic conformational change in the linker2 sequence of PABP and/or the potential shielding of the PABP–PABP interaction site in RRM3 induced by poly(A) binding may contribute to the inhibition of the formation of PABP homodimer.

The inhibition of the PABP–PABP interaction by poly(A)$_{25}$ was unanticipated as the CTD, which does not interact with poly(A), is sufficient for protein-protein interactions (Figure 2C). Indeed, the interaction between CTDs (Flag-C and GST-C), which do not contain an RNA-binding domain, was not inhibited upon the addition of poly(A)$_{25}$ (comparing lanes 4–7 in Figure 3B). Interestingly, the interaction between the CTD of PABP (GST-C) and full-length PABP (Flag-PABP), which contained RNA-binding domains, was completely inhibited upon the addition of poly(A)$_{25}$ (Figure 3C, comparing lanes 4–7 in Figure 3B). We speculate that the poly(A) RNA bound to RRMs inhibit the interaction between CTDs either by putative steric hindrance or by a putative conformational change of the protein-protein interaction site within the CTD. Further investigation is required to determine the molecular basis of this unusual phenomenon. Collectively, our data suggest that two PABP molecules interact with each other to form a homodimer in the absence of poly(A), and the protein-protein interaction is disrupted upon the association of PABP with poly(A) RNA.

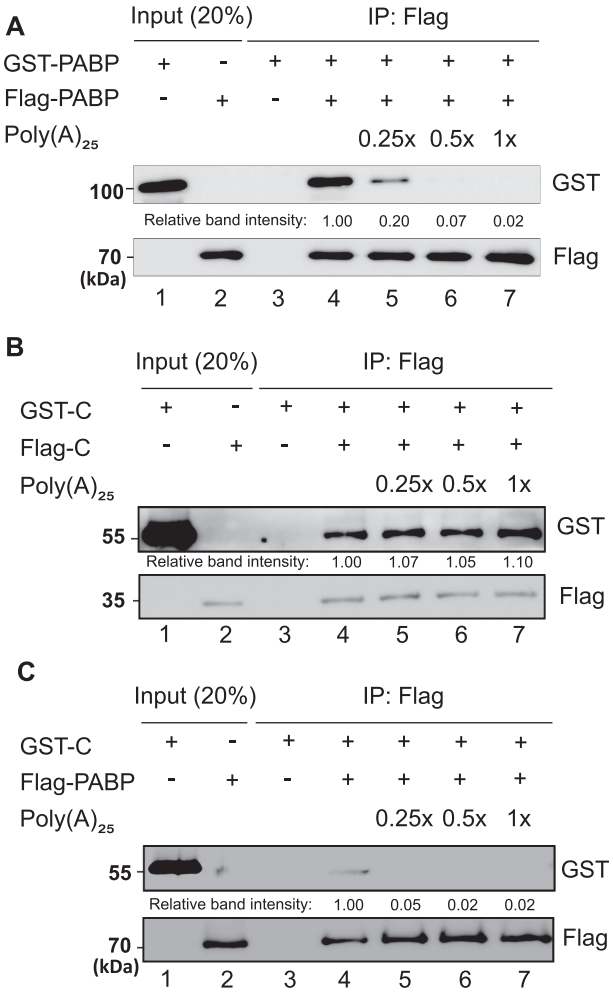

Figure 3. Poly(A) RNA disrupts PABP–PABP interaction. (**A**) The effect of poly(A)$_{25}$ RNA on the PABP–PABP interaction was examined by Flag-immunoprecipitation in the presence of increasing amounts of poly(A)$_{25}$ RNA. Flag-PABP and GST-PABP proteins were incubated together with a Flag resin, and unbound proteins washed away once. Increasing amounts of poly(A)$_{25}$ RNAs up to the concentration of total PABP proteins (represented as 1 x) were added to the mixtures and incubated again. The resin-bound proteins were visualized by Western blotting using the indicated antibodies. (**B**) The effect of poly(A)$_{25}$ RNA on the interaction between GST-C and Flag-C was examined by Flag-immunoprecipitation in the presence of increasing amounts of poly(A)$_{25}$ RNA similarly to panel (**A**). (**C**) The effect of poly(A)$_{25}$ RNA on the interaction between GST-C and Flag-PABP was examined by Flag-immunoprecipitation in the presence of increasing amounts of poly(A)$_{25}$ RNA similarly to panel (A).

Generation of a PABP mutant that tends to dimerize

To investigate the role of PABP dimerization in translational activation, we generated a PABP mutant that affects the interaction between PABP molecules. We focused on the linker2 region as it is essential for PABP homodimerization (Figure 2). Notably, the linker2 region (residues 176–189) is one of the most phylogenetically conserved regions in PABP (Figure 4A). It is composed of consecutive positively and negatively charged residues, which are highly conserved, and more than half of which are charged. We tested the effects of the changes in the negatively charged residues (glutamate (E)), as the positively charged residues could potentially interact with the poly(A) sequence. Among the several mutants tested, a PABP mutant with glutamate (*E*)-to-alanine (A) substitutions at the four glutamate residues in the linker2 region (referred to as PABP 4EA) exerted a strong effect on PABP homodimerization (Figure 4). First, purified Flag-PABP 4EA proteins formed a prominent dimer peak (134 kDa, 13.65 ml) and a very small

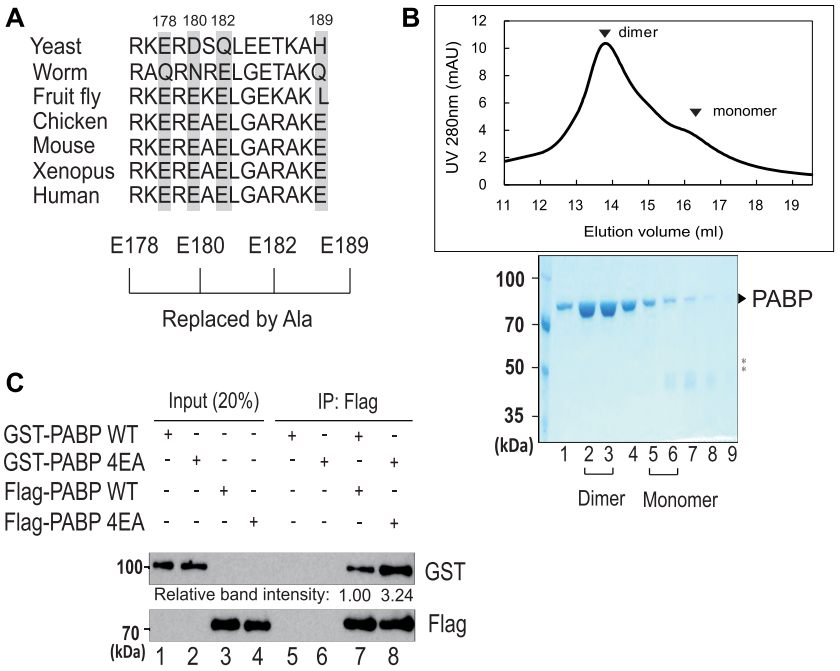

Figure 4. Mutations of four glutamates (Es) to alanines (As) in the linker2 region increase the RNA-free PABP–PABP interaction. (**A**) Sequence alignment of linker2 region of PABP homologs from diverse organisms. Four negatively-charged glutamates (E178, E180, E182, E189) in the linker2 region were mutated to alanines. (**B**) Homo-dimerization of PABP 4EA mutant protein. Size exclusion chromatography was performed with Flag-PABP 4EA mutant proteins as described in Figure 1A. Upper panel: Gel filtration profile of 4EA mutant PABPs. The positions of dimeric and monomeric PABPs are depicted by arrowheads. Lower panel: The proteins in each fraction resolved by 10% SDS-PAGE and stained by Coomassie Blue. The bands depicted by asterisk (*) are likely either bacterial proteins co-purified with PABP or fragment(s) of PABP generated during the purification steps. (**C**) The interaction between 4EA mutant proteins was greatly increased compared with the interaction between PABP WTs. Co-immunoprecipitation experiments were performed with GST-PABP WT and Flag-PABP WT pair or with GST-PABP 4EA mutant and Flag-PABP 4EA mutant pair using a flag antibody-conjugated resin to isolate wild type PABP (lane 7) and 4EA mutant PABP complexes (lane 8), respectively.

monomer peak (52 kDa, 15.81 mL) (Figure 4B). Second, the tendency of dimerization of PABP WT and PABP 4EA was also tested in Co-IP experiments. GST-PABP WT and GST-PABP 4EA co-precipitated with Flag-PABP WT and Flag-PABP 4EA, respectively (lanes 7 and 8 in Figure 4C). In contrast, the negative control Flag resin did not precipitate either GST-PABP WT or GST-PABP 4EA (lanes 5 and 6 in Figure 4C). Importantly, Flag-PABP 4EA proteins co-precipitated by the corresponding pair was approximately 3-fold greater than that of Flag-PABP WT co-precipitated by the corresponding pair (comparing lane 8 with lane 7 in Figure 4C). The results indicate that PABP 4EA exhibits a stronger dimerization tendency than PABP WT.

The PABP–PABP interaction interferes with the PABP-eIF4G interaction

The interaction between PABP and eIF4G, the latter being a scaffold protein that connects PABP with eIF3/eIF4A and the m^7G cap-binding protein eIF4E to promote translation initiation, is necessary for the translational activation function of PABP (35). To investigate the effect of PABP dimerization on translation, we investigated the effect of strengthened PABP dimerization on eIF4G binding to PABP. We compared the binding of eIF4G to PABP WT and PABP 4EA in the presence or absence of poly(A) in Co-IP experiments. In the experiments, we used a truncated human eIF4GI containing PABP- and eIF4E-binding domains (residues 42–653 of eIF4GI, designated as eIF4GN) owing to the technical challenges in the purification of full-length human eIF4GI protein (17). In the absence of poly(A), eIF4GN bound to PABP 4EA was ∼3-fold lower than that of eIF4GN bound to PABP WT (compare lane 6 with lane 5 in Figure 5A). This result indicates that the PABP–PABP interaction weakens the eIF4G-PABP interaction in the absence of poly(A) RNA. Conversely, eIF4GN that was co-precipitated with PABP 4EA bound to poly(A) using a poly(A) RNA resin (Sepharose resin conjugated with ∼100 nt long poly(A)) was the same as that of eIF4GN that co-precipitated with PABP WT bound to poly(A) (comparing lane 7 with lane 8 in Figure 5B). These results indicate that eIF4G exhibits the same affinities for RNA-bound PABP 4EA and RNA-bound PABP WT. Based on these results, we speculate that the eIF4G-binding site, present in the RRM2 of PABP (26), is shielded, at least in part, in a PABP homodimer, even though it is present outside the PABP–PABP interaction domains (linker2-RRM3 and linker of CTD). It implies that the conformational change in PABP induced by poly(A) binding is a prerequisite for promoting the binding of eIF4G to PABP. In fact, we previously reported that the poly(A)-binding of PABP induces a major conformational change in the linker2 region (28), which is necessary for the interaction with eIF4G (17). Therefore, the conformational change induced at the linker2 region upon poly(A)-binding appears to lead to two events: 1) Dissociation of the PABP homodimer, and 2) association of eIF4G with

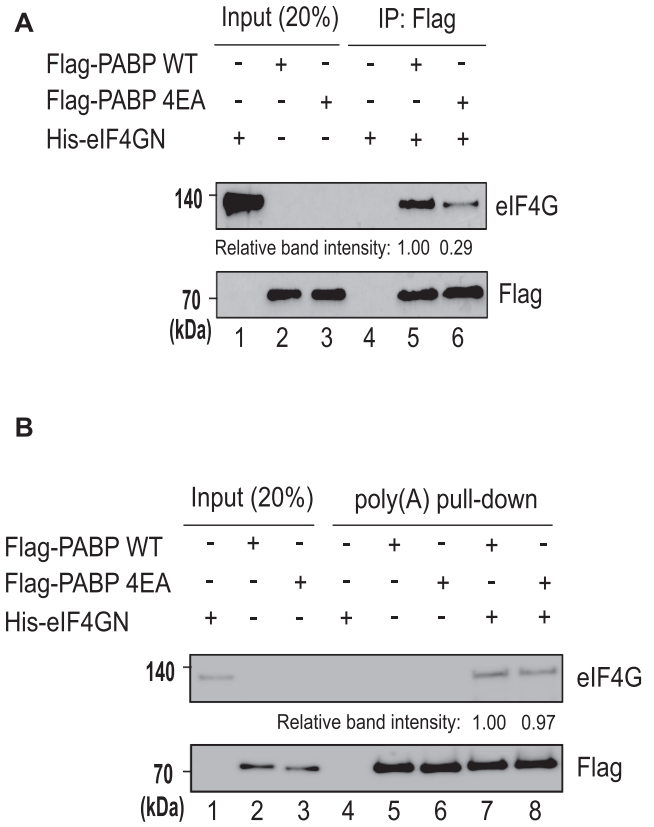

Figure 5. Protein-protein interaction between eIF4G and PABP WT or 4EA mutant. (**A**) The interaction between eIF4G and RNA-free PABPs. Flag-PABP WT or Flag-PABP 4EA proteins were incubated with a Flag resin, and then incubated with His-eIF4GN proteins. His-eIF4GN proteins associated with Flag-PABP WT (lane 5) or Flag-PABP 4EA proteins (lane 6) were visualized by Western blotting with an anti-eIF4G antibody. (**B**) The interaction between eIF4G and poly(A)-bound PABPs. Poly(A) pull-down experiments were performed with His-eIF4GN proteins and either Flag-PABP WT (lane 7) or Flag-PABP 4EA (lane 8) proteins. Resin bound proteins were visualized by Western blotting with the indicated antibodies.

poly(A)-bound PABP. Through these events, eIF4G preferentially binds to poly(A)-bound PABPs rather than to RNA-free PABPs existing as homodimers.

Increased PABP–PABP interaction inhibits the transition of a PABP homodimer to a PABP–poly(A) complex

We found that the poly(A) binding of PABP leads to the inhibition of the PABP dimerization (Figure 3). To assess whether the increased interaction between PABP molecules affects the interaction of PABP with poly(A) RNA or *vice versa*, we investigated the PABP–PABP interaction between PABP 4EA mutants in the presence of increasing concentrations of poly(A)$_{25}$ (Figure 6A). For this experiment, GST-PABP 4EA and Flag-PABP 4EA proteins were purified, and the PABP–PABP interactions were studied using Co-IP with a Flag antibody-conjugated resin. Increasing concentrations of poly(A)$_{25}$ RNA was added (up to the concentration of total PABP proteins (referred to as 1×)), and GST-PABP 4EA co-precipitated by Flag-PABP 4EA was measured using Western blotting. The interaction between PABP 4EA mutants decreased gradually with the addition of increasing concentrations of poly(A)$_{25}$ RNA; however, the decreasing extent of interaction between PABP 4EA mutants by poly(A) RNA was considerably less significant than that of PABP WT (comparing lanes 4–7 of Figures 3A and 6A). In case of PABP WT, the PABP–PABP interaction was remarkably suppressed upon the addition of a low concentration of poly(A)$_{25}$. Approximately 81% reduction was observed upon the addition of 0.25 × poly(A)$_{25}$ RNA, and almost no PABP–PABP interaction was observed when 0.5× poly(A)$_{25}$ was added to the reaction mixture (Figure 3A). On the contrary, in case of PABP 4EA, only 19% reduction of the PABP–PABP interaction was observed when 0.25× poly(A)$_{25}$ RNA was added, and 27% PABP–PABP interaction was retained even after the addition of 1× poly(A)$_{25}$ RNA (lanes 4–7 in Figure 6A). This result indicates that PABP 4EA molecules, which contain mutations that augment PABP–PABP interaction, exhibits a lower tendency of conversion from PABP homodimer to poly(A)–PABP complex in the presence of poly(A) RNA.

We measured the binding affinities of PABP WT and PABP 4EA to poly(A)$_{25}$ using EMSA (Figure 6B). We calculated the K_D values of the PABP–poly(A)$_{25}$ RNA interaction by measuring the disappearance of radioactivity at the free poly(A)$_{25}$ RNA band position. The K_D values of PABP WT and PABP 4EA with poly(A)$_{25}$ RNA were ∼0.5 and ∼2.2 nM, respectively. It indicates that PABP WT exhibits a higher affinity than PABP 4EA to a short poly(A) RNA, which allows the binding of a single PABP molecule. Notably, the supershift in RNA (denoted as *) was shown when PABP proteins were added at a high concentration (Figure 6B). We speculate that more than one PABP molecule may be associated with the poly(A)$_{25}$ RNA, possibly through a PABP–PABP interaction. The supershift in response to a high PABP concentration was observed in both PABP WT and PABP 4EA (Figure 6B). Interestingly, the supershift band appeared firstly at 64 and 16 nM of PABP WT and PABP 4EA, respectively. The supershift at a lower concentration of PABP 4EA compared with PABP WT is likely attributed to slower transition from dimer to monomer of PABP 4EA, as shown in Co-IP experiments (Figures 3A and 6A). Taken together, these results indicate that increased PABP–PABP interaction partially hampers poly(A) binding and the transition from the RNA-free dimer to the poly(A)–PABP complex.

The transition of a PABP homodimer to a poly(A)–PABP complex is necessary for the translational activation function of PABP

To investigate whether the homodimerization of PABP affects its translation activation function, we performed *in vitro* translation experiments using PABP-depleted RRLs supplemented with purified PABP WT or PABP 4EA proteins (Figure 7B). Endogenous PABPs were depleted from RRLs by incubating the lysates with GST-Paip2-conjugated glutathione Sepharose beads, as described previously (38). Lysates incubated with GST-conjugated beads were used as a control. We confirmed the depletion of endogenous PABPs from RRLs by Western blotting using a PABP antibody (Figure 7A). In PABP-depleted lysates, the

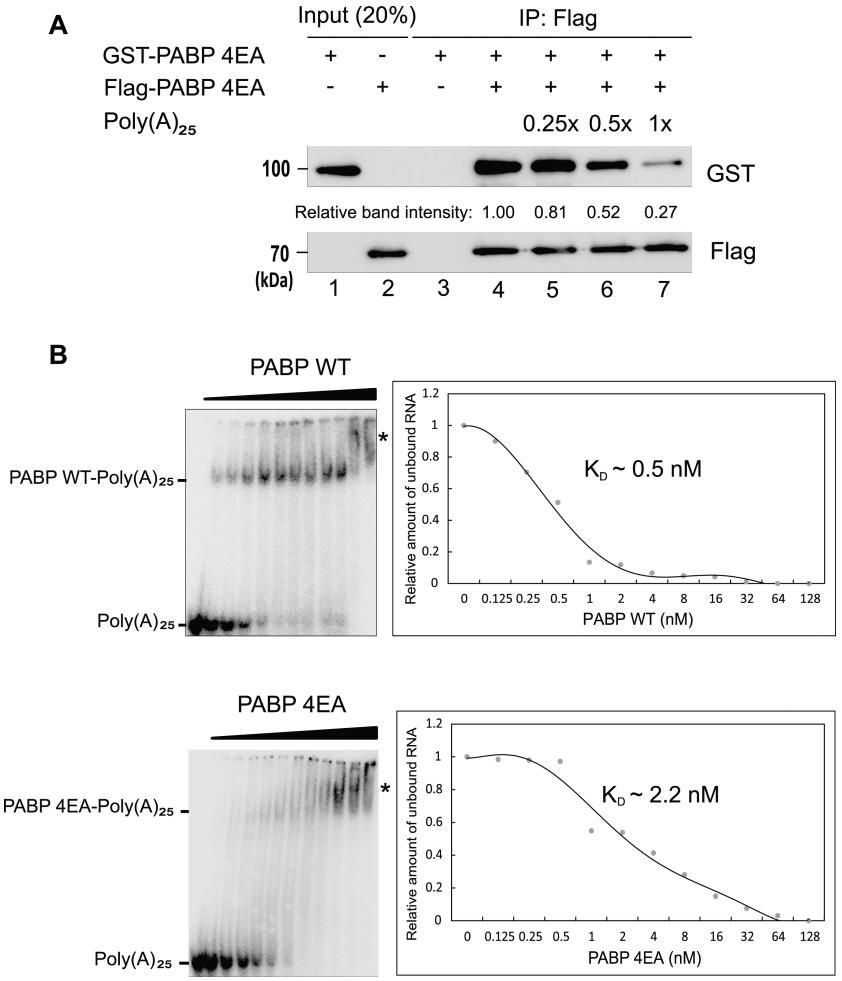

Figure 6. Transition from PABP homo-dimer to poly(A)–PABP complex is hampered by increased PABP–PABP homo-dimer interaction. (**A**) Dissociation of the PABP 4EA-PABP 4EA homo-dimer by poly(A)$_{25}$ RNA. Flag-immunoprecipitation experiments were performed similarly to Figure 3A, except that Flag-PABP 4EA and GST-PABP 4EA were used instead of Flag-PABP WT and GST-PABP WT in these experiments. Resin bound proteins were visualized by Western blotting with the indicated antibodies. (**B**) PABP 4EA has a lower binding affinity than PABP WT to poly(A)$_{25}$ RNA. Electrophoretic mobility shift assays were performed with radiolabeled [^{32}P]-poly(A)$_{25}$ RNA (1 nM) and serially increasing amounts of Flag-PABP WT or Flag-PABP 4EA mutant proteins in the range from 125 pM to 256 nM. (Left panel) A representative image of 6% native acrylamide gel showing an upper-shift of radiolabeled poly(A)$_{25}$ probes through associations with PABP proteins. The asterisks (*) depict the supershift bands of radiolabeled poly(A)$_{25}$ probes at high concentrations of PABP WT and 4EA proteins. (Right panel) The graph shows the radioactivities remained at the protein-free poly(A)$_{25}$ RNA band. The binding affinity (K_D value) was calculated with the remaining radioactivity of protein-free poly(A)$_{25}$ probes on each lane.

translation efficiency of a 5′-m^{7}G capped and 3′-poly(A)$_{120}$-tailed mRNA of the *Renilla* luciferase gene decreased drastically compared to that in undepleted lysates (∼80% reduction; comparing the white columns in Figure 7B). This result indicates that PABP plays a key role in translation. To determine whether the translational efficiency can be recovered by supplementation with PABP WT or PABP 4EA, *in vitro* translation reactions were performed in PABP-depleted lysates after adding PABP WT or PABP 4EA proteins at various concentrations (25 to 100 ng). Upon the addition of WT PABP proteins, translation was gradually recovered with up to ∼73% of undepleted lysates when 50 ng PABP WT proteins were added (black columns in Figure 7B). On the contrary, in PABP 4EA protein-supplemented lysates, the translational efficiencies were restored only up to ∼48% of that in undepleted lysates (hatched columns in Figure 7B). Moreover, we monitored the effect of incubation time (20 min - 80 min) on translation efficiency (Supplementary Figure S7). The difference between PABP WT and PABP 4EA in augmenting translation reactions was clearly observed at different time points (20, 40, 60 and 80 min), but the patterns of translation efficiencies with the supplementations of PABP WT or PABP 4EA were very similar to each other at different time points (Supplementary Figure S7A–E). Notably, the highest translational efficiencies were observed when the PABP-depleted lysates were supplemented with 50 ng of PABP WT or PABP 4EA proteins. Afterwards, the translational efficiencies decreased when proteins were added at higher concentrations. By measuring the level of endogenous PABP in the control lysate using Western blotting (Figure 7C), we found that the reaction mixture of control lysates (denoted by 1×) contains ∼60 ng of PABP proteins, similar to the concentration of supplemented PABP that exhibited the highest translational

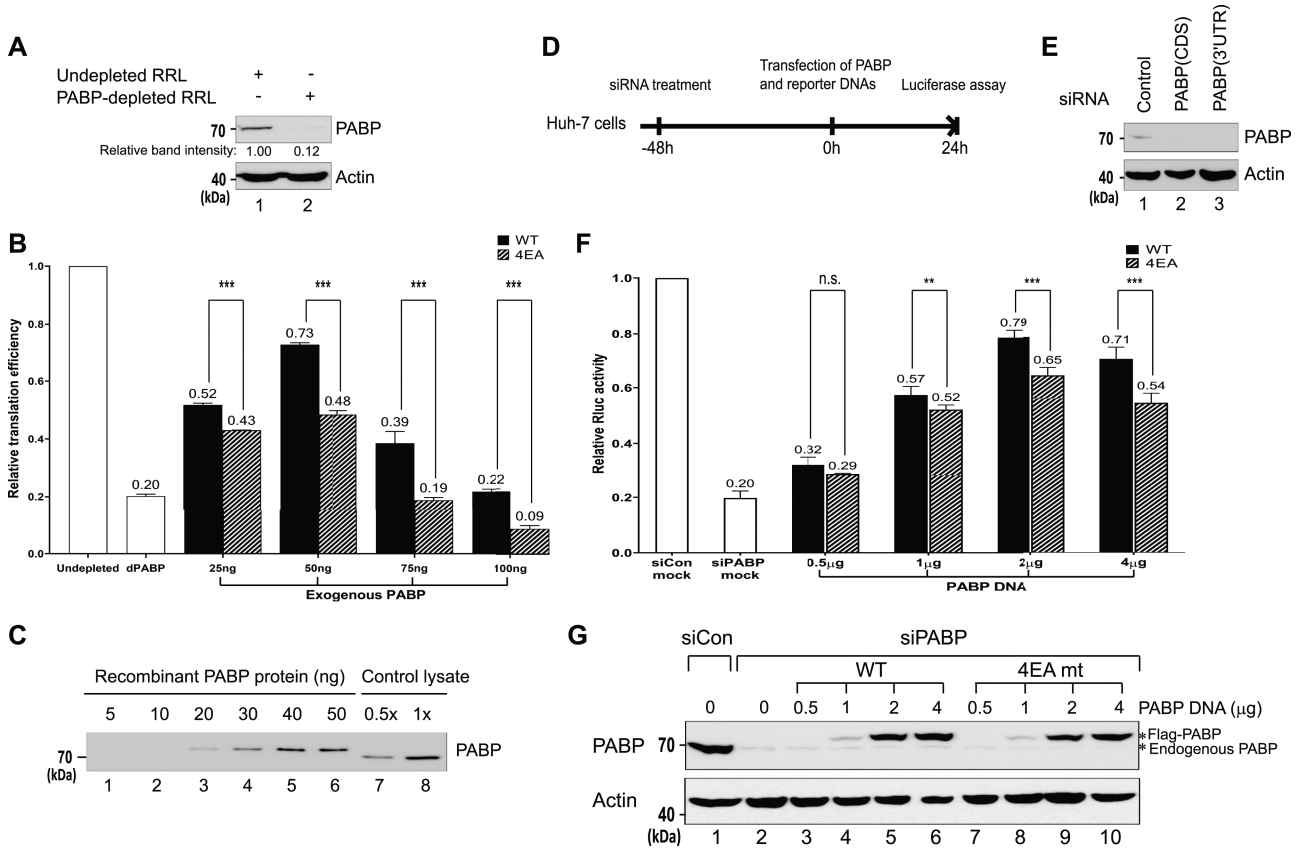

Figure 7. Proper transition from a PABP homo-dimer to a poly(A)–PABP complex is required for translational activation function of PABP. (**A**) Depletion of endogenous PABP from rabbit reticulocyte lysates was confirmed by Western blotting of control and PABP-depleted lysates with an anti-PABP antibody. Actin was used as a control protein. (**B**) *In vitro* translation assays were performed using the PABP-depleted lysates supplemented with various amounts of PABP WT or PABP 4EA proteins from 0 ng to 100 ng for 60 min. *In vitro* transcription was executed by T7 RNA polymerase with a template DNA containing the *Renilla* luciferase gene followed by poly(A)$_{120}$ sequence to produce 5′ capped and 3′ poly(A)-tailed mRNAs. Relative translational efficiencies were calculated by normalizing translational efficiencies of the reporter mRNAs with various amounts of PABP WT or PABP 4EA to that in PABP-undepleted control lysates which was set to 1. The relative translational efficiencies are depicted by the bar graphs. The white columns denoted as undepleted and dPABP represent relative translation efficiencies of PABP-undepleted control and PABP-depleted lysates, respectively. The black and hatched columns represent translation efficiencies of PABP-depleted lysates supplemented with PABP WT and PABP 4EA, respectively. *In vitro* translation reactions were performed three times to acquire statistical values. The columns and bars represent the means and ± standard deviations, respectively. The average value is depicted on the top of each column. P values less than 0.001 are given three asterisks (***). The amounts of supplemented proteins are depicted on the x-axis. (**C**) The amount of endogenous PABP proteins in the PABP-undepleted control lysates was estimated by Western blotting with the control lysates and purified PABP proteins of known concentrations. The amount of lysates used in one *in vitro* translation reaction is denoted as 1x. (**D**) Schematic diagram of experimental design of *in cellulo* assays. Endogenous PABPs in Huh-7 cells were knocked-down by treatment of a siRNA targeting 3′UTR of PABP mRNA. After 48 h treatment, effector DNAs (0–4 μg) containing PABP WT or PABP 4EA genes were transfected into the Huh-7 cells. Reporter DNAs containing the *Renilla* luciferase gene were co-transfected with the effector DNAs to monitor translation efficiency of a capped and polyadenylated mRNA. At 24 h after the DNA transfection, cells were lysed and luciferase activities in the lysates were measured. (**E**) Knock-down efficiency of endogenous PABPs in Huh-7 cells was monitored by Western blotting using an anti-PABP antibody. Dramatic decrease of PABP levels was observed by both siRNAs targeting the coding sequence (lane 2) and 3′UTR (lane 3) of PABP. A control siRNA was used as a negative control (lane 1). (**F**) Luciferase assays were performed using PABP-depleted Huh-7 cells after the ectopic expression of PABP WT or PABP 4EA proteins. Relative translational efficiencies were calculated by normalizing luciferase activities in cells expressing various amounts of PABP WT or PABP 4EA to that in siCon cells which was set to 1. The graphs are drawn as described in panel (B). *P* values less than 0.001 are given three asterisks (***), and *P* values less than 0.01 are given two asterisks (**). *P* values higher than 0.05 are given non-significant (n.s.). (**G**) The knock-down of endogenous PABP and the ectopic expression (*Flag-PABP) of PABP WT and PABP 4EA in transfected cells were monitored by Western blotting using an anti-PABP antibody.

activation function (Figure 7B). The addition of PABP at concentrations greater than the endogenous PABP concentration suppressed the translation of mRNAs. This finding is consistent with that from a previous study, according to which excess PABP represses the translation of mRNAs *via* unknown mechanisms (34).

To test whether similar phenomena occur in cells, we conducted luciferase reporter assays using PABP-knockdown cells transfected with DNA encoding PABP WT or PABP 4EA (Figure 7D). An siRNA targeting the 3′UTR of PABP was transfected into Huh-7 cells to knockdown endogenous PABP mRNAs. However, this siRNA did not interfere with the expression of ectopically produced PABP WT and PABP 4EA mRNAs lacking the 3′UTR of endogenous PABP mRNA. After transfection with the siRNA for 48 h, the cells were transfected with DNA encoding 3× Flag-tagged PABP WT or PABP 4EA (0.5–4 μg) along with a DNA reporter encoding *Renilla* luciferase (Rluc).

At 24 h from the DNA transfection, the cells were lysed, and the Rluc activity in the lysates was measured to examine translational recovery by ectopically expressed PABP WT and PABP 4EA. We confirmed that endogenous PABP expression was almost completely knocked down by siRNAs targeting the 3′UTR and the coding sequence of PABP (39) (Figure 7E). Compared to that in the control siRNA-transfected cells, translation was decreased by approximately 80% in the siPABP-transfected cells (white columns in Figure 7F), similar to PABP depletion observed in the *in vitro* translation assay (white columns in Figure 7B). Transfection with increasing concentrations of PABP WT DNA (up to 2 μg) gradually enhanced translation, followed by inhibition (black columns in Figure 7F). This indicates that ectopic PABP WT expression restores the *in vivo* translation of reporter mRNAs. Transfection with PABP 4EA DNA also enhanced the translation of reporter mRNAs, but the extent of translational enhancement was lower than that achieved with PABP WT DNA (hatched columns in Figure 7F). The levels of PABP WT and PABP 4EA proteins were monitored by Western blotting (Figure 7G), and the levels of reporter RNA were monitored by quantitative RT-PCR (Supplementary Figure S8). These results indicate that the conversion of the PABP homodimer to the poly(A)–PABP complex is necessary for its translational activation function.

DISCUSSION

Here, we report that PABP forms a homodimer without poly(A) *via* direct protein-protein interactions. Using purified PABP derivatives spanning different parts of PABP, we revealed that PABP homodimerization is mediated by two independent regions: (i) linker2-RRM3 (designated as HIR1) and (ii) the Linker in CTD (designated as HIR2). HIR1 interacts with HIR1, and HIR2 interacts with HIR2, indicating that the interactions in the two molecules of PABP lead to a head-to-head (or tail-to-tail) configuration of the RNA-free PABP dimer. This model is partly consistent with a previous report suggesting that the CTD is involved in PABP–PABP interaction (43). Full-length PABP was shown to co-precipitate with [^{35}S]-labeled full-length PABP and the CTD of PABP (43). However, our PABP dimer model was inconsistent with that described in another previous report on the PABP–PABP interaction (41). The authors reported that [^{35}S]-labeled PABP co-precipitated only with the RRM3-4-a partial CTD of PABP (residues 237–542), but not with GST-1–2–3–4, CTD, or full-length PABP protein (41). The discrepancy in the results is interesting because the authors adopted similar approaches in the investigations of the domains responsible for PABP–PABP interaction (41,43). This discrepancy could be attributed to the complexity of the testing system. Both research groups used *in vitro* translation systems containing several proteins and RNAs that may have interfered with or augmented the PABP–PABP interaction. Moreover, the proteins in RRL could non-specifically bind to resins conjugated with various GST-fused PABP proteins (41). To minimize the complexity of the experiments owing to the presence of cellular proteins and RNAs, we investigated the PABP–PABP interaction and identified the domains responsible for the interaction using purified polypeptides corresponding to various parts of PABP. Using this approach, we identified a new region in PABP responsible for the PABP–PABP interaction, designated as HIR1, in addition to the Linker of CTD designated as HIR2. We tested the interactions between HIR1 and between HIR2 regions under various conditions to rule out the possibility of non-specific interaction observable under specific conditions. We observed the interaction between HIR1s under all conditions tested, but we did not observe the interaction between HIR2s under harsh reaction conditions, such as high detergent concentrations (data not shown). Moreover, we found that the HIR1-HIR1 interaction was stronger than the HIR2-HIR2 interaction under favorable conditions, as shown in Figure 2B, 2C and 2D. The results indicate that HIR1 plays a major role in the PABP–PABP interaction, and HIR2 promotes this interaction.

Our new PABP dimer model is entirely different from the structure of poly(A)-bound Pab1, which is the yeast homolog of PABP (29). Poly(A)-bound Pab1 oligomers exhibit a head-to-tail type of interaction, in which a linker helix extruding from RRM4 contacts the RRM1 region of the adjacent Pab1 molecule on a poly(A) RNA chain (Supplementary Figure 1) (29). Since the orientation and intermolecular interactions of PABPs in RNA-free and poly(A)-bound forms are completely different from each other, we attempted to investigate how RNA-free PABP dimers are converted to poly(A)-bound PABP oligomers. Examination of the effect of poly(A) on the PABP–PABP homodimer revealed that the PABP–PABP interaction was inhibited upon the addition of poly(A)$_{25}$ RNA. This indicates that the PABP–PABP homodimer dissociates into monomers, at least transiently, before forming the more stable PABP–poly(A) complex. It is plausible that the binding of RRM1–RRM2 of PABP to poly(A), which does not participate in PABP–PABP homodimerization and exhibit a considerably high binding affinity to poly(A) RNA (K_D of RRM1–RRM2 with poly(A) is 2 nM (15,16)), induces a conformational change in linker2, which in turn prevents the HIR1-HIR1 interaction. However, we cannot rule out the possibility that the putative poly(A)–RRM3 interaction affects HIR1-HIR1 interaction even though the binding affinity of RRM3 to poly(A) is lower than that of RRM1–RRM2 (K_D of RRM3-C with poly(A) was 116 nM (15)). Lastly, it is also possible that the RNA-free monomeric PABP, in equilibrium with the dimeric PABP (Figure 1A), quickly associates with poly(A) in the presence of poly(A), which results in a stable PABP–poly(A) complex. The continuous drainage of monomeric PABP from the pool of RNA-free PABP molecules can eventually result in conversion of RNA-free PABP, in a monomer–dimer equilibrium, to RNA-bound PABP *via* a transient monomeric form. The detailed process of conversion from an RNA-free dimeric PABP to a PABP–poly(A) complex remains to be elucidated.

Several reports have suggested the potential role of the CTD in the cooperative binding of PABP to poly(A) (15,41,42). However, the importance of the cooperative binding of PABP to poly(A) RNA has been challenged by recent reports in which the length of poly(A) tails were measured at the genomic scale using next-generation sequencing (31,32). The authors suggested that the median length

of the human poly(A) tail is approximately 60 nucleotides (31,32). Considering that the footprint of a single PABP on poly(A) RNA is approximately 25 nucleotides, a single cellular mRNA is considered to be likely occupied by two PABP molecules on an average. This indicates that an RNA-free PABP dimer can cover the poly(A) tail of an mRNA.

Considering the concentrations of mRNAs and translation initiation factors (PABP, eIF4G, and eIF4E) and the binding affinities (K_D) among them, it is most likely that translational initiation commences with the interaction between the poly(A) tail and PABP, followed by sequential interactions in the order of 3′-poly(A)–PABP-eIF4G-eIF4E-5′ m^7G cap, as described in the Introduction. Therefore, the interaction between PABP and the poly(A) tail and the subsequent interaction between poly(A)-bound PABP and eIF4G are the key steps in translation. In contrast, eIF4E knockdown did not affect the global translation (data not shown), which is consistent with findings from previous reports (11–13). This suggests that translation initiation can occur even in the absence of eIF4E. Some eIF4E-independent translations are likely to occur *via* the alternative m^7G cap-binding protein eIF3d for the translation of specific mRNAs, such as c-*Jun* mRNA (46,47). In addition, internal ribosome entry sites (IRESs), which exist in approximately 10% of cellular mRNAs (48,49), may direct the translation of IRES-containing cellular mRNAs in an eIF4E-independent manner. In fact, IRES-dependent translation was discovered through investigations of the translation mechanism of naturally uncapped viral mRNAs. IRES elements were first identified in the 5′UTRs of encephalomyocarditis virus (EMCV) and poliovirus (both picornaviruses) RNAs (50,51). Another type of IRES element was identified in the 5′UTR of hepatitis C virus RNA (52). All of the three IRES elements lack the m^7G cap structure, existing in most eukaryotic mRNAs, do not require the m^7G cap structure for translation activation function as indicated by the name of the translation element. However, interestingly, a subset of eIF4F (eIF4A and eIF4G but not eIF4E) is needed for the IRES-dependent translation of EMCV and poliovirus mRNAs.

The mechanism by which the poly(A) tail enhances the translation of mRNAs that lack an IRES element or a specialized eIF3d-binding sequence in m^7G cap-independent manner remains unknown. We may be able to find clues for the mechanism from another type of virus that produces naturally uncapped mRNAs. Most positive-strand RNA plant viruses lack the 5′-m^7G cap and/or the poly(A)-tail. Several of them lack the 5′ m^7G cap structure but contain a translation-enhancing element at the 3′UTR, named m^7G cap-independent translation enhancer (CITE). CITEs recruit 40S ribosomal subunits either directly *via* a CITE-ribosome interaction or indirectly by interacting with a translation factor (such as eIF4G and eIF4E) (53). The 40S ribosome, which is recruited to a CITE present at the 3′UTR, may communicate with the 5′ region of the mRNA through long-range RNA-RNA interaction between the putative ‘kissing loop’. However, the kissing loop interaction was shown to be unnecessary for some CITE-mediated translations, even though the mechanism underlying the identification of the initiation codon by the 40S ribosome on the 3′UTR without kissing loop interaction remains unknown (53). An interesting example of poly(A)-dependent but 5′ m^7G cap-independent translation related to this phenomenon was reported (9,10). The authors showed that the poly(A) tail could facilitate translation of the upstream gene even in the absence of the 5′ m^7G cap structure. This indicates that the 40S ribosome recruited at the 3′UTR of an mRNA by the poly(A) tail can execute translation without assistance from the m^7G cap structure. More recently, a systematic analysis of translation mediated by 40S ribosomes recruited to various parts of an mRNA was reported using *in vitro* and *in cellulo* assay systems (54). The authors showed that the 40S ribosomes, which were recruited to the 3′UTRs of uncapped mRNAs either by the insertion of the EMCV IRES element or by the tethering of eIF4G to MS2-binding sites, could enhance the translation of a reporter gene located upstream of the ribosome recruitment sites. Based on these observations and the findings from other biochemical and molecular biological studies, the authors proposed that the recognition of the initiation codon by a 40S ribosome recruited to an mRNA can occur *via* the biased stochastic collision of the 40S ribosome with the initiation codon through RNA looping of the intervening region rather than *via* ribosome scanning (54,55). The hypothesis of the direct recognition of the initiation codon by an mRNA-bound 40S ribosome was supported by the structural analysis of the 48S translation initiation complex, which revealed the positions of the mRNA, $tRNA_i^{Met}$, eIF2, and several subunits of eIF3, eIF4A and eIF4G on the 40S ribosomal subunit (56). Based on the structure of the 48S complex, the direct slotting of mRNAs to the 40S ribosome was proposed as a likely mechanism to form the specific configuration of the 48S translational initiation complex (56). The authors recognized that the slotting model is compatible with the translation of circular mRNAs (57) as well as the initiation of mRNAs containing IRES elements. We suggest that the slotting model can be applied to translational enhancement by the poly(A) tail. To slot the translation initiation site of an mRNA to the 40S ribosome recruited on the poly(A) tail, mRNA looping should occur in a biased stochastic manner, which would be affected by the distance between the 40S ribosome-recruitment site and the initiation site, the structure of the intervening sequence, and other factors.

In conclusion, our work revealed the configuration of RNA-free PABPs that do not participate in translation activation. We determined how idling PABPs, which exist at considerably higher cellular concentrations than eIF4G, do not interfere with translation by sequestering eIF4G. In other words, we showed that the drastic conformational change of PABPs induced by the binding of poly(A) RNA exposes the binding sites for eIF4G that remain unexposed in the RNA-free PABP homodimer. Our findings may help improve our understanding of the mechanism underlying the transition of RNA-free PABPs to poly(A)-bound PABPs.

DATA AVAILABILITY

All data are available in the main text or the Supplementary Data.

SUPPLEMENTARY DATA

Supplementary Data are available at NAR Online.

FUNDING

This research was supported by Bio & Medical Technology Development Program of the National Research Foundation (NRF) funded by the Korean government (MSIT) [NRF-2019M3E5D6063871]. Funding for open access charge: Pohang University of Science and Technology (POSTECH).
Conflict of interest statement. None declared.

REFERENCES

1. Gallie,D.R. (1991) The cap and poly(A) tail function synergistically to regulate mRNA translational efficiency. *Genes Dev.*, **5**, 2108–2116.
2. Tarun,S.Z. Jr. and Sachs,A.B. (1996) Association of the yeast poly(A) tail binding protein with translation initiation factor eIF-4G. *EMBO J.*, **15**, 7168–7177.
3. Tarun,S.Z. Jr., Wells,S.E., Deardorff,J.A. and Sachs,A.B. (1997) Translation initiation factor eIF4G mediates in vitro poly(A) tail-dependent translation. *Proc. Natl. Acad. Sci. U.S.A.*, **94**, 9046–9051.
4. Wells,S.E., Hillner,P.E., Vale,R.D. and Sachs,A.B. (1998) Circularization of mRNA by eukaryotic translation initiation factors. *Mol. Cell*, **2**, 135–140.
5. Imataka,H., Gradi,A. and Sonenberg,N. (1998) A newly identified N-terminal amino acid sequence of human eIF4G binds poly(A)-binding protein and functions in poly(A)-dependent translation. *EMBO J.*, **17**, 7480–7489.
6. Borman,A.M., Michel,Y.M. and Kean,K.M. (2000) Biochemical characterisation of cap-poly(A) synergy in rabbit reticulocyte lysates: the eIF4G-PABP interaction increases the functional affinity of eIF4E for the capped mRNA 5′-end. *Nucleic Acids Res.*, **28**, 4068–4075.
7. Tarun,S.Z. Jr. and Sachs,A.B. (1995) A common function for mRNA 5′ and 3′ ends in translation initiation in yeast. *Genes Dev.*, **9**, 2997–3007.
8. Iizuka,N., Najita,L., Franzusoff,A. and Sarnow,P. (1994) Cap-dependent and cap-independent translation by internal initiation of mRNAs in cell extracts prepared from *Saccharomyces cerevisiae*. *Mol. Cell. Biol.*, **14**, 7322–7330.
9. Preiss,T., Muckenthaler,M. and Hentze,M.W. (1998) Poly(A)-tail-promoted translation in yeast: implications for translational control. *RNA*, **4**, 1321–1331.
10. Preiss,T. and Hentze,M.W. (1998) Dual function of the messenger RNA cap structure in poly(A)-tail-promoted translation in yeast. *Nature*, **392**, 516–520.
11. Rau,M., Ohlmann,T., Morley,S.J. and Pain,V.M. (1996) A reevaluation of the cap-binding protein, eIF4E, as a rate-limiting factor for initiation of translation in reticulocyte lysate. *J. Biol. Chem.*, **271**, 8983–8990.
12. Yanagiya,A., Suyama,E., Adachi,H., Svitkin,Y.V., Aza-Blanc,P., Imataka,H., Mikami,S., Martineau,Y., Ronai,Z.A. and Sonenberg,N. (2012) Translational homeostasis via the mRNA cap-binding protein, eIF4E. *Mol. Cell*, **46**, 847–858.
13. Truitt,M.L., Conn,C.S., Shi,Z., Pang,X., Tokuyasu,T., Coady,A.M., Seo,Y., Barna,M. and Ruggero,D. (2015) Differential requirements for eIF4E dose in normal development and cancer. *Cell*, **162**, 59–71.
14. Gorlach,M., Burd,C.G. and Dreyfuss,G. (1994) The mRNA poly(A)-binding protein: localization, abundance, and RNA-binding specificity. *Exp. Cell Res.*, **211**, 400–407.
15. Kuhn,U. and Pieler,T. (1996) Xenopus poly(A) binding protein: functional domains in RNA binding and protein-protein interaction. *J. Mol. Biol.*, **256**, 20–30.
16. Sladic,R.T., Lagnado,C.A., Bagley,C.J. and Goodall,G.J. (2004) Human PABP binds AU-rich RNA via RNA-binding domains 3 and 4. *Eur. J. Biochem.*, **271**, 450–457.
17. Hong,K.Y., Lee,S.H., Gu,S., Kim,E., An,S., Kwon,J., Lee,J.B. and Jang,S.K. (2017) The bent conformation of poly(A)-binding protein induced by RNA-binding is required for its translational activation function. *RNA Biol*, **14**, 370–377.
18. Karim,M.M., Svitkin,Y.V., Kahvejian,A., De Crescenzo,G., Costa-Mattioli,M. and Sonenberg,N. (2006) A mechanism of translational repression by competition of Paip2 with eIF4G for poly(A) binding protein (PABP) binding. *Proc. Natl. Acad. Sci. U.S.A.*, **103**, 9494–9499.
19. Friedland,D.E., Wooten,W.N., LaVoy,J.E., Hagedorn,C.H. and Goss,D.J. (2005) A mutant of eukaryotic protein synthesis initiation factor eIF4E(K119A) has an increased binding affinity for both m7G cap analogues and eIF4G peptides. *Biochemistry*, **44**, 4546–4550.
20. O'Leary,S.E., Petrov,A., Chen,J. and Puglisi,J.D. (2013) Dynamic recognition of the mRNA cap by *Saccharomyces cerevisiae* eIF4E. *Structure*, **21**, 2197–2207.
21. Slepenkov,S.V., Darzynkiewicz,E. and Rhoads,R.E. (2006) Stopped-flow kinetic analysis of eIF4E and phosphorylated eIF4E binding to cap analogs and capped oligoribonucleotides: evidence for a one-step binding mechanism. *J. Biol. Chem.*, **281**, 14927–14938.
22. Kentsis,A., Topisirovic,I., Culjkovic,B., Shao,L. and Borden,K.L. (2004) Ribavirin suppresses eIF4E-mediated oncogenic transformation by physical mimicry of the 7-methyl guanosine mRNA cap. *Proc. Natl. Acad. Sci. U.S.A.*, **101**, 18105–18110.
23. Kulak,N.A., Pichler,G., Paron,I., Nagaraj,N. and Mann,M. (2014) Minimal, encapsulated proteomic-sample processing applied to copy-number estimation in eukaryotic cells. *Nat. Methods*, **11**, 319–324.
24. Khaleghpour,K., Kahvejian,A., De Crescenzo,G., Roy,G., Svitkin,Y.V., Imataka,H., O'Connor-McCourt,M. and Sonenberg,N. (2001) Dual interactions of the translational repressor Paip2 with poly(A) binding protein. *Mol. Cell. Biol.*, **21**, 5200–5213.
25. Xie,J., Kozlov,G. and Gehring,K. (2014) The "tale" of poly(A) binding protein: the MLLE domain and PAM2-containing proteins. *Biochim. Biophys. Acta*, **1839**, 1062–1068.
26. Safaee,N., Kozlov,G., Noronha,A.M., Xie,J., Wilds,C.J. and Gehring,K. (2012) Interdomain allostery promotes assembly of the poly(A) mRNA complex with PABP and eIF4G. *Mol. Cell*, **48**, 375–386.
27. Deo,R.C., Bonanno,J.B., Sonenberg,N. and Burley,S.K. (1999) Recognition of polyadenylate RNA by the poly(A)-binding protein. *Cell*, **98**, 835–845.
28. Lee,S.H., Oh,J., Park,J., Paek,K.Y., Rho,S., Jang,S.K. and Lee,J.B. (2014) Poly(A) RNA and Paip2 act as allosteric regulators of poly(A)-binding protein. *Nucleic Acids Res.*, **42**, 2697–2707.
29. Schafer,I.B., Yamashita,M., Schuller,J.M., Schussler,S., Reichelt,P., Strauss,M. and Conti,E. (2019) Molecular basis for poly(A) RNP architecture and recognition by the Pan2-Pan3 deadenylase. *Cell*, **177**, 1619–1631.
30. Duncan,R. and Hershey,J.W. (1983) Identification and quantitation of levels of protein synthesis initiation factors in crude HeLa cell lysates by two-dimensional polyacrylamide gel electrophoresis. *J. Biol. Chem.*, **258**, 7228–7235.
31. Subtelny,A.O., Eichhorn,S.W., Chen,G.R., Sive,H. and Bartel,D.P. (2014) Poly(A)-tail profiling reveals an embryonic switch in translational control. *Nature*, **508**, 66–71.
32. Chang,H., Lim,J., Ha,M. and Kim,V.N. (2014) TAIL-seq: genome-wide determination of poly(A) tail length and 3′ end modifications. *Mol. Cell*, **53**, 1044–1052.
33. Khaleghpour,K., Svitkin,Y.V., Craig,A.W., DeMaria,C.T., Deo,R.C., Burley,S.K. and Sonenberg,N. (2001) Translational repression by a novel partner of human poly(A) binding protein, Paip2. *Mol. Cell*, **7**, 205–216.
34. Kini,H.K., Vishnu,M.R. and Liebhaber,S.A. (2010) Too much PABP, too little translation. *J. Clin. Invest.*, **120**, 3090–3093.
35. Kahvejian,A., Svitkin,Y.V., Sukarieh,R., M'Boutchou,M.N. and Sonenberg,N. (2005) Mammalian poly(A)-binding protein is a eukaryotic translation initiation factor, which acts via multiple mechanisms. *Genes Dev.*, **19**, 104–113.
36. Punjani,A., Rubinstein,J.L., Fleet,D.J. and Brubaker,M.A. (2017) cryoSPARC: algorithms for rapid unsupervised cryo-EM structure determination. *Nat. Methods*, **14**, 290–296.
37. Rohou,A. and Grigorieff,N. (2015) CTFFIND4: Fast and accurate defocus estimation from electron micrographs. *J. Struct. Biol.*, **192**, 216–221.

38. Svitkin,Y.V., Yanagiya,A., Karetnikov,A.E., Alain,T., Fabian,M.R., Khoutorsky,A., Perreault,S., Topisirovic,I. and Sonenberg,N. (2013) Control of translation and miRNA-dependent repression by a novel poly(A) binding protein, hnRNP-Q. *PLoS Biol.*, **11**, e1001564.
39. Yoshida,M., Yoshida,K., Kozlov,G., Lim,N.S., De Crescenzo,G., Pang,Z., Berlanga,J.J., Kahvejian,A., Gehring,K., Wing,S.S. *et al.* (2006) Poly(A) binding protein (PABP) homeostasis is mediated by the stability of its inhibitor, Paip2. *EMBO J.*, **25**, 1934–1944.
40. Bustin,S.A., Benes,V., Garson,J.A., Hellemans,J., Huggett,J., Kubista,M., Mueller,R., Nolan,T., Pfaffl,M.W., Shipley,G.L. *et al.* (2009) The MIQE guidelines: minimum information for publication of quantitative real-time PCR experiments. *Clin. Chem.*, **55**, 611–622.
41. Melo,E.O., Dhalia,R., Martins de Sa,C., Standart,N. and de Melo Neto,O.P. (2003) Identification of a C-terminal poly(A)-binding protein (PABP)-PABP interaction domain: role in cooperative binding to poly (A) and efficient cap distal translational repression. *J. Biol. Chem.*, **278**, 46357–46368.
42. Lin,J., Fabian,M., Sonenberg,N. and Meller,A. (2012) Nanopore detachment kinetics of poly(A) binding proteins from RNA molecules reveals the critical role of C-terminus interactions. *Biophys. J.*, **102**, 1427–1434.
43. Patel,G.P. and Bag,J. (2006) IMP1 interacts with poly(A)-binding protein (PABP) and the autoregulatory translational control element of PABP-mRNA through the KH III-IV domain. *FEBS J.*, **273**, 5678–5690.
44. Mangus,D.A., Evans,M.C. and Jacobson,A. (2003) Poly(A)-binding proteins: multifunctional scaffolds for the post-transcriptional control of gene expression. *Genome Biol.*, **4**, 223.
45. Baer,B.W. and Kornberg,R.D. (1980) Repeating structure of cytoplasmic poly(A)-ribonucleoprotein. *Proc. Natl. Acad. Sci. U.S.A.*, **77**, 1890–1892.
46. Lee,A.S., Kranzusch,P.J., Doudna,J.A. and Cate,J.H. (2016) eIF3d is an mRNA cap-binding protein that is required for specialized translation initiation. *Nature*, **536**, 96–99.
47. Lamper,A.M., Fleming,R.H., Ladd,K.M. and Lee,A.S.Y. (2020) A phosphorylation-regulated eIF3d translation switch mediates cellular adaptation to metabolic stress. *Science*, **370**, 853–856.
48. Wellensiek,B.P., Larsen,A.C., Stephens,B., Kukurba,K., Waern,K., Briones,N., Liu,L., Snyder,M., Jacobs,B.L., Kumar,S. *et al.* (2013) Genome-wide profiling of human cap-independent translation-enhancing elements. *Nat. Methods*, **10**, 747–750.
49. Weingarten-Gabbay,S., Elias-Kirma,S., Nir,R., Gritsenko,A.A., Stern-Ginossar,N., Yakhini,Z., Weinberger,A. and Segal,E. (2016) Comparative genetics. Systematic discovery of cap-independent translation sequences in human and viral genomes. *Science*, **351**, aad4939.
50. Jang,S.K., Krausslich,H.G., Nicklin,M.J., Duke,G.M., Palmenberg,A.C. and Wimmer,E. (1988) A segment of the 5′ nontranslated region of encephalomyocarditis virus RNA directs internal entry of ribosomes during in vitro translation. *J. Virol.*, **62**, 2636–2643.
51. Pelletier,J. and Sonenberg,N. (1988) Internal initiation of translation of eukaryotic mRNA directed by a sequence derived from poliovirus RNA. *Nature*, **334**, 320–325.
52. Tsukiyama-Kohara,K., Iizuka,N., Kohara,M. and Nomoto,A. (1992) Internal ribosome entry site within hepatitis C virus RNA. *J. Virol.*, **66**, 1476–1483.
53. Truniger,V., Miras,M. and Aranda,M.A. (2017) Structural and functional diversity of plant virus 3′-Cap-independent translation enhancers (3′-CITEs). *Front Plant Sci*, **8**, 2047.
54. Paek,K.Y., Hong,K.Y., Ryu,I., Park,S.M., Keum,S.J., Kwon,O.S. and Jang,S.K. (2015) Translation initiation mediated by RNA looping. *Proc. Natl. Acad. Sci. U.S.A.*, **112**, 1041–1046.
55. Jang,S.K. and Paek,K.Y. (2016) Cap-dependent translation is mediated by 'RNA looping' rather than 'ribosome scanning'. *RNA Biol*, **13**, 1–5.
56. Brito Querido,J., Sokabe,M., Kraatz,S., Gordiyenko,Y., Skehel,J.M., Fraser,C.S. and Ramakrishnan,V. (2020) Structure of a human 48S translational initiation complex. *Science*, **369**, 1220–1227.
57. Yang,Y., Fan,X., Mao,M., Song,X., Wu,P., Zhang,Y., Jin,Y., Yang,Y., Chen,L.L., Wang,Y. *et al.* (2017) Extensive translation of circular RNAs driven by N(6)-methyladenosine. *Cell Res.*, **27**, 626–641.